JCTC Journal of Chemical Theory and Computation

pubs.acs.org/JCTC Article

Quantum Simulation of Molecular Response Properties in the NISQ Era

Ashutosh Kumar,* Ayush Asthana, Vibin Abraham, T. Daniel Crawford, Nicholas J. Mayhall, Yu Zhang,* Lukasz Cincio, Sergei Tretiak, and Pavel A. Dub*

Cite This: J. Chem. Theory Comput. 2023, 19, 9136−9150

ABSTRACT: Accurate modeling of the response of molecular systems to an external electromagnetic field is challenging on classical computers, especially in the regime of strong electronic correlation. In this article, we develop a quantum linear response (qLR) theory to calculate molecular response properties on near-term quantum computers. Inspired by the recently developed variants of the quantum counterpart of equation of motion (qEOM) theory, the qLR formalism employs "killer condition" satisfying excitation operator manifolds that offer a number of theoretical advantages along with reduced quantum resource requirements. We also used the qEOM framework in this work to calculate the state-specific response properties. Further, through noiseless quantum simulations, we show that response properties calculated using the qLR approach are more accurate than the ones obtained from the classical coupled-cluster-based linear response models due to the improved quality of the ground-state wave function obtained using the ADAPT-VQE algorithm.

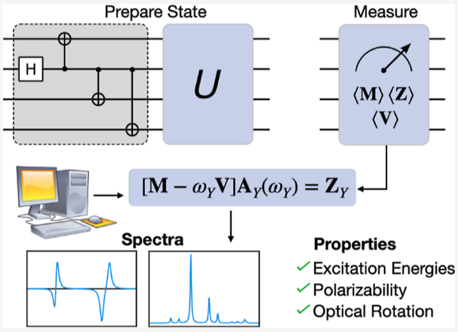

INTRODUCTION

The field of quantum chemistry has made significant progress in recent decades in the accurate numerical simulation of electronic properties of a wide range of molecules and materials.[1−5] However, a number of challenges still remain. The computational complexity of accurate electronic structure methods continues to be quite high, especially when strong electron correlation effects are involved, where the numerical evaluation of the ground and low-lying excited states of the molecular Hamiltonian may scale factorially with respect to the system size.[6] With the advent of quantum devices that exploit the quantum properties of superposition and entanglement, one can map the exponentially increasing Hilbert space to a linearly scaling number of qubits.[7] The quantum hardware in the NISQ era, however, suffers from a number of challenges like limited qubit connectivity, significant gate-error rates, short coherence times, etc., which prevent us from realizing the promised "quantum advantage". The variational eigensolver (VQE) method[8] attempts to overcome some of these limitations by ensuring shallow quantum circuits through a variational optimization of the quantum circuit parameters. This has allowed for the development of a number of quantum algorithms for the simulation of molecular ground[8−24] and excited states.[25−34] Aside from the VQE method, algorithms based on quantum phase estimation,[35,36] adiabatic state preparation,[37,38] and Krylov subspace generation[39−41] have also been developed for molecular simulations. These techniques are more suitable for the era of fault-tolerant quantum computing.

Most of the quantum computing applications in chemistry have been focused on the estimation of ground- and excited-state energies with limited attention to molecular response properties. As the name suggests, these properties capture the response of the electric dipole moment of a molecule to an external field. For example, the molecular polarizability is defined as the first-order response of the electronic charge distribution to an external electric field. Polarizabilities are at the origin of many chemical phenomena including electron scattering,[42] electronegativity,[43] and softness and hardness,[44] and they play an important role in biological processes such as protein−ligand binding.[45] When strong electric fields are involved, as in the case of lasers, higher-order response properties such as hyperpolarizabilities (second-order) also become significant. These quantities, for example, define the suitability of materials for nonlinear optical applications.[46] Chiroptical properties are another class of response properties that have found several applications in the pharmaceutical industry. More than half of the drugs currently in use are

Received: July 2, 2023
Revised: October 29, 2023
Accepted: October 31, 2023
Published: December 6, 2023

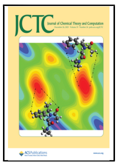

https://doi.org/10.1021/acs.jctc.3c00731

chiral,[47] i.e., the molecular structure of these drugs has a unique three-dimensional handedness and thus exists in the form of left- and right-hand stereoisomers, also known as enantiomers. Within a chiral environment, the chemical properties of the enantiomers can be drastically different. This underscores the importance of understanding the structure−activity relationship of these compounds.[48] Optical rotation, which refers to the rotation of the plane of plane-polarized light as it passes through a chiral medium, is a useful tool for determining the absolute configuration of chiral molecular systems. Just like polarizabilities, optical rotation can be characterized as the first-order response of the electric dipole moment but with respect to an external magnetic field.

The exact treatment of these response properties can be carried out by the sum-over-states (SoS) formalism,[49] which involves explicit evaluation of all the excited states associated with the molecular Hamiltonian. Consequently, implementing the SoS approach for even medium-sized molecular systems can be challenging. An alternative approach is built on the idea of expanding the perturbed wave functions in a determinantal basis rather,[49−52] thus avoiding the explicit determination of the excited states. In classical quantum chemistry, coupled-cluster (CC) response theory (RT), developed extensively by Koch, Jörgensen, and co-workers,[49,51,52] is one of the most promising approaches in this regard. Another popular approach is through the use of equation of motion coupled cluster (EOM-CC) theory introduced by Stanton and Bartlett.[53] Unlike the CC-RT formalism, this method attempts to calculate response properties within the SoS framework based on excited states computed using EOM-CC. Green's function-based approaches[54,55] are yet another class of methods that are frequently used to calculate the molecular response properties. It should be noted that excitation energies (EEs) and transition moments generally also come under the purview of the response properties. Since both of these properties are state-specific, they can be calculated efficiently by both CC-RT- and EOM-CC-based approaches.

Important recent developments have been made in computing response properties on a quantum computer.[56−62] The variational quantum response (VQR) algorithm developed by Huang and co-workers[56] is notable in this regard. The VQR approach transforms the response formalism into an optimization problem that minimizes a cost function using a parameterized quantum circuit to calculate dipole polarizabilities and absorption spectra. A number of recently developed quantum excited-state methods like subspace-search VQE (SS-VQE),[25] the orthogonal state reduction variational eigensolver (OSRVE),[26] and variational quantum deflation (VQD)[27,28] operate on similar principles with appropriately designed cost functions for excited-state energies. Although these methods are promising, they suffer from challenges like increased circuit complexity, and there may be additional challenges finding the global minimum in different cost-function optimization landscapes.[63] Alternatively, excited states can also be obtained by diagonalizing the Hamiltonian in a subspace, just like the classical EOM-CC-based approaches. Quantum equation of motion (qEOM)[33] and quantum subspace expansion (QSE)[29−32] methods are popular examples in this regard. These methods have the same circuit complexity as the ground state but feature an increase in the number of measurements and higher body reduced density matrix (RDM) requirements. However, the qEOM approach does not necessarily satisfy the important "killer" or vacuum annihilation condition (VAC),[64,65] while the QSE approach does not guarantee the correct scaling (size-intensivity[66,67]) of energy differences. The q-sc-EOM approach developed by us recently[34] satisfies the "killer" condition by making use of the self-consistent excitation manifold[64] of Mukherjee. Further, it transforms the generalized non-Hermitian eigenvalue problem of qEOM into a Hermitian eigenvalue problem, provides size-intensive energy differences, and is expected to be more noise-resilient compared to other diagonalization-based excited state approaches.

In this work, we propose a new formalism, namely, quantum linear response (qLR) theory to simulate molecular response properties such as polarizabilities, optical rotation, etc., on near-term quantum computers.[68] The ground-state wave function in qLR theory can be obtained from any VQE-based algorithm, which makes this approach NISQ compatible. Consistent with the classical linear RT, in the qLR approach, one needs to solve a perturbation-dependent linear system of equations to evaluate the response properties. The difference lies in the fact that all of the elements of the matrices and vectors appearing in the equations are now measured on a quantum computer instead. To the best of our knowledge, there has been no implementation of UCC-based linear RT in the field of classical quantum chemistry to date for calculating higher-order response properties. This can be attributed to a series of intricate approximations that need to be developed due to the nontruncating nature of the Hausdorff expansion for UCC-based methods.[69] Of course, no such approximations are needed for a quantum simulation, and hence, the qLR theory can help shed some light toward the practical development of such approaches in classical quantum chemistry as well. We also make use of the "killer condition" satisfying operator manifolds in this work, which ensure that accurate response properties are obtained with reduced quantum resource requirements. Furthermore, the quantum equation-of-motion framework developed in refs 34 and 70 was utilized for the quantum simulation of state-specific response properties like transition moments and EEs. This article is structured as follows: The Theory section discusses the theoretical formalism for the qLR theory. The Vacuum Annihilation or "Killer" Condition section introduces the "killer condition" and operator manifolds that ensure that this condition is always satisfied, which is then used to derive the final qLR working equations. The proposed implementation steps are shown in the Proposed Implementation section, while the computational details for all the calculations in this paper are reported in the Computational Details section. The Results section discusses the results obtained for H_2, LiH, H_2O, chiral $(H_2)_2$, and linear H_6 molecular systems. The key findings of this article are summarized in the Conclusions section. For completeness, the Appendix sections presents some aspects of linear RT and the theoretical framework of the qEOM method.

■ THEORY

Linear Response Theory. Molecular RT captures the interaction of a molecule with an external electromagnetic field based on the time-dependent perturbation theory framework, starting from the time-dependent Schrödinger equation

$$\hat{H}|\Psi_0(t)\rangle = i\frac{d}{dt}|\Psi_0(t)\rangle \tag{1}$$

Using perturbation theory, the Hamiltonian is partitioned into a zeroth-order component, which describes the molecule in the absence of any time-dependent field, and a first-order component, which is the semiclassical interaction between the molecule and an external dynamic field

$$\hat{H}(t) = \hat{H}^{(0)} + \hat{H}^{(1)}(t) \tag{2}$$

There are two principal formalisms for calculating response properties. The first involves the expansion of the time-dependent wave function and the corresponding expectation-value properties, such as the electric dipole moment, in orders of the perturbation, followed by Fourier transformation to the frequency domain, yielding order-by-order property tensors such as the polarizability, optical activity tensor, etc.[49] (see the Appendix for details.) The second approach identifies response functions as derivatives of the time-averaged quasi-energy with respect to external field strength parameters.[51,71] We make use of the latter formalism in this work. The quasi-energy formalism was first introduced by Sasagane[71] and later refined by Hättig, Christiansen, and Jörgensen.[51]

We can express the first-order perturbation component of the Hamiltonian in eq 2 as a discrete sum of periodic perturbations as

$$\hat{H}^{(1)}(t) = \sum_{j=-N}^{j=N} e^{-i\omega_j t}\hat{H}^{(1)}(\omega_j),\ \hat{H}^{(1)}(\omega_j) = \sum_{Y} \varepsilon_Y(\omega_j)\hat{Y} \tag{3}$$

where $\hat{Y}$ is a frequency-independent operator describing the interaction between the external field and the molecular system and ϵ_Y is the frequency-dependent strength parameter associated with the given external field (see ref 51), while N refers to the total number of monochromatic periodic perturbations. For example, $\hat{Y}$ corresponds to the dipole moment operator $(\vec{\mu})$ when the perturbation is an oscillating electric field and is associated with the magnetic moment operator $(\vec{m})$ in the case of an external magnetic field. This can be expressed in the second quantized formalism as

$$\hat{Y} = Y_q^p a_p^\dagger a_q \tag{4}$$

where Y_q^p refers to $\langle \chi_p | \vec{\mu}_i | \chi_q \rangle$ with $i \in \{x, y, z\}$ in the case of an external electric field and $\langle \chi_p | \vec{m}_i | \chi_q \rangle$ for a magnetic field. The indices p and q denote the molecular orbitals and the operators $a_p^\dagger$ and a_q are the usual Fermionic creation and annihilation operators. It should be noted that $\vec{\mu}_i = -\vec{r}_i$ and $\vec{m}_i = -\frac{1}{2}(\vec{r} \times \vec{p})_i$, where $\vec{r}$ and $\vec{p}$ refer to the position and momentum vectors, respectively. Thus, the summation over in eq 3 covers all the possible interactions of the molecular system with a given external field. To ensure that $\hat{H}^{(1)}(t)$ stays Hermitian, the operator $\hat{Y}$ should be Hermitian as well, along with other necessary conditions such as $\omega_{-j} = -\omega_j$ and $\varepsilon_Y^*(\omega_j) = \varepsilon_Y(-\omega_j)$.

The central quantity in this quasi-energy formalism is the time-dependent quasi-energy defined as

$$Q(t) = \langle \Psi_0(t) | \left(\hat{H}^{(0)} + \hat{H}^{(1)}(t) - i\frac{d}{dt} \right) | \Psi_0(t) \rangle \tag{5}$$

The quasi-energy can be seen as an analogue of energy in the time-dependent domain. By invoking the time-averaged time-dependent Hellmann–Feynman theorem,[51] one can obtain response functions by taking the derivatives of the time-averaged quasi-energy with respect to external field strength parameters.

In order to derive the response equations, we consider the following time-dependent ansatz of the wave function in the presence of an external field

$$|\Psi_0(t)\rangle = e^{\hat{R}(t)}|\Psi_0\rangle \tag{6}$$

where the $\hat{R}(t)$ is linear cluster operator of the following form

$$\hat{R}(t) = \hat{R}_1(t) + \hat{R}_2(t) + \hat{R}_3(t) + \dots \tag{7}$$

The ground-state $|\Psi_0\rangle$ here is the optimized ground-state wave function obtained by a VQE algorithm on a quantum computer. We define the operators $\hat{R}_i$ $(i \in \{1, 2, 3, ..\})$ using second-quantized excitation and de-excitation operators of the ith rank as

$$\hat{R}_i(t) = \sum_{\mu} [A_{\mu_i}(t)\hat{G}_{\mu_i} + A^*_{\mu_i^\dagger}(t)\hat{G}_{\mu_i^\dagger}] \tag{8}$$

where $\hat{G}_{\mu_i}$ and $\hat{G}_{\mu_i^\dagger}$ refer to an excitation and de-excitation operator of rank i with the corresponding response amplitudes $A_{\mu i}(t)$ and $A^*_{\mu_i^\dagger}(t)$, respectively. The value of i can, of course, range from 1 to N, where N is the number of electrons in the system. The action of these operators on the reference wave function $|0\rangle$—Hartree–Fock (HF) in our case—can be illustrated mathematically as

$$\hat{G}_{\mu_i}|0\rangle = |\mu_i\rangle$$

$$\langle 0|\hat{G}_{\mu_i^\dagger} = \langle \mu_i| \tag{9}$$

where $|\mu_i\rangle$ denotes an "excited" Slater determinant of rank i. One can expand the Fourier components of these response amplitudes in successive orders of the perturbation, just like in eq A.2 in the Appendix. It can be shown that solving the time-dependent Schrödinger equation is equivalent to the variational minimization of the time-averaged quasi-energy, which is defined as $\{L(t)\}_T = \frac{1}{T}\int_0^T dt\ Q(t)$.[51] After expanding the quasi-energy in different orders of the perturbation $(L(t) = L^{(0)}(t) + L^{(1)}(t) + L^{(2)}(t) + ...)$, the equations for solving frequency-dependent response amplitudes of different orders can be obtained through the following equations

$$\frac{\partial}{\partial A_{\mu_i}^{(m)}(\omega_j)}\{L^{(n)}(t)\}_T = 0$$

$$\frac{\partial}{\partial A_{\mu_i}^{(m)*}(\omega_j)}\{L^{(n)}(t)\}_T = 0 \tag{10}$$

where $m \leq n$. It should be noted that the response amplitudes satisfy the $2n + 1$ rule, which states that for calculating a molecular property of perturbation order $2n + 1$, one needs only up to order n wave function parameters. Thus, first-order response amplitudes can provide up to third-order properties, such as hyperpolarizabilities. Putting $m = 1$, $n = 2$ in eq 10, one obtains the following secular equation for first-order response amplitudes associated with the perturbation operator $\hat{Y}$ at frequency ω_j

$$\left[\begin{pmatrix} \mathbf{M} & \mathbf{Q} \\ \mathbf{Q}^* & \mathbf{M}^* \end{pmatrix} - \omega_j \begin{pmatrix} \mathbf{V} & \mathbf{W} \\ -\mathbf{W}^* & -\mathbf{V}^* \end{pmatrix}\right]\begin{bmatrix} \mathbf{A}_Y^{(1)}(\omega_j) \\ \mathbf{B}_Y^{(1)}(\omega_j) \end{bmatrix} = \begin{bmatrix} \mathbf{Z}_Y \\ -\mathbf{Z}_Y^* \end{bmatrix} \tag{11}$$

where $\mathbf{B}_Y^{(1)} = (\mathbf{A}_Y^{(1)})^\dagger$ and the elements of matrices **M**, **Q**, **V**, **W**, and vector $\mathbf{G}_\mathbf{Y}$ are defined as

$$\begin{aligned} \mathrm{M}_{\mu_i,\nu_j} &= \langle \Psi_0 | [\hat{G}_{\mu_i^\dagger}, [\hat{H}, \hat{G}_{\nu_j}]] | \Psi_0 \rangle \\ \mathrm{V}_{\mu_i,\nu_j} &= \langle \Psi_0 | [\hat{G}_{\mu_i^\dagger}, \hat{G}_{\nu_j}] | \Psi_0 \rangle \\ \mathrm{Q}_{\mu_i,\nu_j} &= -\langle \Psi_0 | [\hat{G}_{\mu_i^\dagger}, [\hat{H}, \hat{G}_{\nu_j^\dagger}]] | \Psi_0 \rangle \\ \mathrm{W}_{\mu_i,\nu_j} &= -\langle \Psi_0 | [\hat{G}_{\mu_i^\dagger}, \hat{G}_{\nu_j^\dagger}] | \Psi_0 \rangle \\ Z_Y(\mu_i) &= \langle \Psi_0 | [\hat{\mathrm{Y}}, \hat{G}_{\mu_i}] | \Psi_0 \rangle \end{aligned} \tag{12}$$

Finally, the response functions can be obtained by taking the derivative of the time-averaged quasi-energy of an appropriate order with respect to field strengths. For example, the linear response function can be obtained as

$$\begin{aligned} \langle\langle X; Y \rangle\rangle_{\omega_j} &= \frac{\partial^2 \{L^{(2)}(t)\}_T}{\partial \varepsilon_X(-\omega_j) \partial \varepsilon_Y(\omega_j)} \\ &= \mathbf{Z}_\mathbf{X} \cdot \mathbf{A}_Y(\omega_j) + \mathbf{Z}_\mathbf{X}^* \cdot \mathbf{B}_Y(\omega_j) \end{aligned} \tag{13}$$

where $Z_X(\boldsymbol{\mu}_i) = \langle \Psi_0 | [\hat{X}, \hat{G}_{\mu_i}] | \Psi_0 \rangle$ and $\cdot$ refers to the dot product operation. For exact electronic states, the linear response function can also be written as a SoS expression[49]

$$\langle\langle X; Y \rangle\rangle_{\omega_j} = \sum_{k>0} \frac{\langle \Psi_0 | \hat{X} | \Psi_k \rangle \langle \Psi_k | \hat{Y} | \Psi_0 \rangle}{\omega_j - \omega_k} - \sum_{k>0} \frac{\langle \Psi_0 | \hat{Y} | \Psi_k \rangle \langle \Psi_k | \hat{X} | \Psi_0 \rangle}{\omega_j + \omega_k} \tag{14}$$

where $\langle \Psi_k |$ refers to the wave function of the kth excited state with the EE of ω_k. Calculation of properties like specific rotation using the SoS formalism can be computationally prohibitive as thousands of electronic excited states may need to be evaluated to ensure the convergence of eq 14.[72] However, the SoS approach has its own advantages as well, especially for resonant and near-resonant responses, where one just needs only excited states within a desired spectral window. The linear response approach avoids the explicit calculation of all excited states by parameterizing the perturbation of the ground-state wave function in the presence of an external field through response amplitudes, which are solved through a linear system of equations. Furthermore, one can also get the values of EEs and transition moments for a given excited state by identifying the poles and evaluating the residues of the linear response function at poles, respectively.[49] It should be noted that the values of EEs, ionization potentials (IPs), and electronic affinities (EAs) calculated using the qLR approach should be identical to the ones obtained from the qEOM approach.[49] Please refer to the Appendix (section) for a detailed theoretical background of the qEOM method. In an earlier work,[34] we have shown that the qEOM method does not necessarily satisfy the "killer condition", leading to large errors for IPs and EAs even for small molecular systems. Thus, one needs to make sure that the qLR approach also complies with the "killer condition" in order to obtain accurate molecular response properties.

Vacuum Annihilation or "Killer" Condition. The VAC states that the ground state cannot be de-excited since it is the lowest-energy eigenstate, i.e.

$$\hat{\mathbb{O}}_k^\dagger | \Psi_0 \rangle = 0 \tag{15}$$

where $\hat{\mathbb{O}}_k$ is a state-transfer operator such that its action on the ground state leads to the kth excited state

$$\hat{\mathbb{O}}_k | \Psi_0 \rangle = | \Psi_k \rangle \tag{16}$$

It is easy to see that the VAC is satisfied for an exact state-transfer operator[64,65,73−76] by writing it in a projector form as

$$\hat{\mathbb{O}}_k = | \Psi_k \rangle \langle \Psi_0 | \tag{17}$$

The application of the adjoint of the exact state-transfer operator on the ground-state wave function produces null, i.e.,

$$\hat{\mathbb{O}}_k^\dagger | \Psi_0 \rangle = | \Psi_0 \rangle \langle \Psi_k | \Psi_0 \rangle = 0 \forall k \tag{18}$$

since the ground- and excited-state wave functions are always orthogonal to each other. However, the VAC may not be satisfied for approximate state-transfer operators. For instance, the VAC is not necessarily satisfied for a general state-transfer operator defined in the qEOM formalism (see eq B.2), i.e.,

$$\hat{\mathbb{O}}_k^\dagger | \Psi_0 \rangle = \sum_i \sum_{\mu_i} [(A^\mathrm{k})^*_{\mu_i^\dagger} \hat{G}_{\mu_i^\dagger} + (B^\mathrm{k})^*_{\mu_i} \hat{G}_{\mu_i}] | \Psi_0 \rangle \neq 0 \tag{19}$$

This can lead to nonorthogonal ground- and excited-state wave functions and produce large errors in charged excitation energies.[34] Two distinct methods were proposed to satisfy the VAC for approximate state-transfer operators, namely, self-consistent operators[64] and projection-based approaches[65] (both discussed below) leading to two different formalisms for estimating excited-state properties.

Self-Consistent Operators. One way to ensure that the VAC is always satisfied is through the use of a self-consistent operator manifold instead of the manifold defined by using HF as the reference. This approach was originally introduced by Prasad and Mukherjee[64] for methods with unitary parameterization of the ground-state wave function. The self-consistent manifold can be defined using the primitive excitation manifold $(\hat{G}_{\mu_i} \cup \hat{G}_{\mu_i^\dagger})$ as

$$\hat{S}_{\mu_i} = U(\theta) \hat{\mathrm{G}}_{\mu_i} U^\dagger(\theta) \tag{20}$$

where $U(\theta)$ refers to the unitary operator used to obtain the ground-state wave function $(| \Psi_0 \rangle)$.

It can be seen that the application of the action of the adjoint of a general-state transfer operator, defined using the operators from the self-consistent operator manifold, on the ground-state wave function is zero, i.e.,

$$\begin{aligned} \mathbb{O}_k^\dagger | \Psi_0 \rangle &= \sum_{\mu_i} (A^k)^*_{\mu_i^\dagger} \mathrm{U}(\theta) \hat{G}_{\mu_i^\dagger} U^\dagger(\theta) \mathrm{U}(\theta) | 0 \rangle \\ &= \sum_{\mu_i} (A^k)^*_{\mu_i^\dagger} \mathrm{U}(\theta) \hat{G}_{\mu_i^\dagger} | 0 \rangle \\ &= 0 \end{aligned} \tag{21}$$

as the regular de-excitation operator acting on the reference wave function yields zero. It should be noted that this formalism is general and applies to any wave function ansatz where the ground state is obtained through an action of a unitary operator acting on a starting state such as HF. Similar approaches have been developed for excited-state methods using unitary coupled-cluster (UCC) theory.[69]

Use of the self-consistent operator manifold in qEOM gives rise to the following simplified working equation

$$\mathbf{M}^{\text{sc}}\mathbf{A}_k = E_{0k}\mathbf{A}_k \tag{22}$$

where

$$\mathrm{M}^{\text{sc}}_{\mu_i,\nu_j} = \langle 0|\hat{G}_{\mu_i^{\dagger}}U^{\dagger}(\theta)\hat{H}U(\theta)\hat{G}_{\nu_j}|0\rangle - \delta_{\mu_i,\nu_j}\cdot \mathrm{E}_0 \tag{23}$$

For more details, please refer to ref 34.

Using the self-consistent operator manifold, the response equations obtained in eq 11 are also simplified and can now be separated into two equations

$$\begin{aligned}(\mathbf{M}^{\text{sc}} - \omega_{\mathrm{Y}}\mathbf{I})\mathbf{A}_{\mathrm{Y}}(\omega_{\mathrm{Y}}) &= \mathbf{Z}^{\text{sc}}_{Y}\\ (\mathbf{M}^{\text{sc}} + \omega_{\mathrm{Y}}\mathbf{I})\mathbf{B}_{\mathrm{Y}}(\omega_{\mathrm{Y}}) &= -\mathbf{Z}^{\text{sc}^*}_{Y}\end{aligned} \tag{24}$$

where $Z^{\text{sc}}_{Y}(\mu_i) = \langle\Psi_0|U^{\dagger}(\theta)\hat{\mathrm{Y}}\mathrm{U}(\theta)\hat{G}_{\mu_i}|\Psi_0\rangle$. However, one can combine the above two equations into one single equation in order to lower the computational costs involved. For example, if we consider the perturbation to be electric-dipole based, $\mathbf{Z}^{\text{sc}}_{\mathrm{Y}}$ is identical to $\mathbf{Z}^{\text{sc}}_{\mathrm{Y}}{}^*$ and we arrive at the following equation

$$((\mathbf{M}^{\text{sc}})^2 - \omega_{\mathrm{Y}}^2\mathbf{I})(\mathbf{A}_{\mathbf{Y}}(\omega_{\mathrm{Y}}) - \mathbf{B}_{\mathbf{Y}}(\omega_{\mathrm{Y}})) = 2\cdot\mathbf{M}^{\text{sc}}\mathbf{Z}^{\text{sc}}_{\mathbf{Y}} \tag{25}$$

and the linear response function can be reformulated as

$$\langle\langle\mathbf{X}, \mathbf{Y}\rangle\rangle_{\omega_{\mathrm{Y}}} = \frac{1}{\omega_{\mathrm{Y}}}\mathbf{Z}^{\text{sc}}_{\mathbf{X}}\cdot(\mathbf{M}^{\text{sc}}(\mathbf{A}_{\mathrm{Y}}(\omega_{\mathrm{Y}}) - \mathbf{B}_{\mathrm{Y}}(\omega_{\mathrm{Y}})) \tag{26}$$

Projection Operators. Surjáan and co-workers developed the projection operator technique[65] to ensure that the VAC is always satisfied while calculating molecular IPs. The projected excitation operator $(\hat{S}_{\mu_i})$ can be written as

$$\hat{S}_{\mu_i} = \hat{G}_{\mu_i}|\Psi_0\rangle\langle\Psi_0| \tag{27}$$

For non-number-conserving operators (which appear in IP or electron affinity calculations), it can be easily seen that the action of the projected de-excitation operator on the ground-state wave function vanishes, i.e.,

$$(\hat{S}_{\mu_i})^{\dagger}|\Psi_0\rangle = |\Psi_0\rangle\langle\Psi_0|\hat{G}_{\mu_i^{\dagger}}|\Psi_0\rangle = 0 \tag{28}$$

Fan and co-workers[70,77] recently made use of these operator manifolds within the framework of equation of motion theory to calculate band structures on a quantum computer. To ensure that eq 28 also holds true for number-conserving operators, we shift all the operators by their expectation values

$$\hat{\hat{G}}_{\mu_i} = \hat{G}_{\mu_i} - \langle\Psi_0|\hat{G}_{\mu_i}|\Psi_0\rangle \tag{29}$$

This can also be seen as a form of a normal ordering of the operators with respect to a general reference wave function.[78] Just like the self-consistent formalism, this approach is quite general and can be used with any wave function ansatz. Using the shifted projected operators in eq B.5 (see the Appendix), one gets a generalized Hermitian eigenvalue equation

$$\mathbf{M}^{\text{proj}}\mathbf{A}_k = E_{0k}\mathbf{V}^{\text{proj}}\mathbf{A}_k \tag{30}$$

where

$$\begin{aligned}M^{\text{proj}}_{\mu_i,\nu_j} &= \langle\Psi_0|\hat{\hat{G}}_{\mu_i^{\dagger}}\hat{\mathrm{H}}\hat{\hat{G}}_{\nu_j}|\Psi_0\rangle\\ V^{\text{proj}}_{\mu_i,\nu_j} &= \langle\Psi_0|\hat{\hat{G}}_{\mu_i^{\dagger}}\hat{\hat{G}}_{\nu_j}|\Psi_0\rangle\end{aligned} \tag{31}$$

Equation 30 looks very similar to the one obtained in the QSE approach, except that the identity operator is not involved in the operator pool. Stated differently, unlike the QSE approach, the ground-state wave function does not participate in the diagonalization procedure, which ensures size-intensive excitation energies. However, the evaluation of the overlap matrix makes it more susceptible to noise,[34] compared to the self-consistent operator approach.

The equations for calculating the response amplitudes are simplified as well when we make use of these shifted projection operators. Equation 12 now can be decoupled into two separate equations

$$\begin{aligned}(\mathbf{M}^{\text{proj}} - \omega_{Y}\mathbf{V}^{\text{proj}})\mathbf{A}_{Y}(\omega_{Y}) &= \mathbf{Z}^{\text{proj}}_{Y}\\ (\mathbf{M}^{\text{proj}} + \omega_{Y}\mathbf{V}^{\text{proj}})\mathbf{B}_{Y}(\omega_{Y}) &= -\mathbf{Z}^{\text{proj}*}_{Y}\end{aligned} \tag{32}$$

where $Z^{\text{proj}}_{Y}(\mu_i) = \langle\Psi_0|\hat{Y}\hat{G}_{\mu_i}|\Psi_0\rangle$. Of course, one can combine the two equations into a single one and obtain equations similar to the self-consistent approach [eq 25] with the identity matrix $\mathbf{I}$ replaced by the overlap matrix $\mathbf{V}^{\text{proj}}$.

PROPOSED IMPLEMENTATION

The qLR forms making use of the self-consistent and projected operator manifolds are referred to as qLR(sc) and qLR(proj), respectively. Here, we discuss the proposed implementation of qLR(sc) and qLR(proj) methods on near-term quantum computers. The working equations of the qLR(sc) method are given in eq 25, which requires the evaluation of matrices $\mathbf{M}^{\text{sc}}$ and $\mathbf{Z}^{\text{sc}}_{\mathbf{Y}}$ on a quantum computer, after which the resulting equation is solved classically. The creation of matrix $\mathbf{M}^{\text{sc}}$ requires the creation of diagonal and off-diagonal terms defined by eq 23. The evaluation of matrix $\mathbf{M}^{\text{sc}}$ can be carried out by the methods discussed in ref 34 without the use of any ancilla qubits. To summarize, the diagonal elements can be evaluated as the expectation value of using the preoptimized circuit obtained during the VQE procedure for estimating the ground-state wave function. However, instead of the HF state, singly and doubly excited Slater determinants are now used as the reference, e.g.,

$$M^{\text{sc}}_{\mu_i,\mu_i} = \langle 0|\hat{G}_{\mu_i^{\dagger}}U^{\dagger}(\theta)\hat{H}U(\theta)\hat{G}_{\mu_i}|0\rangle \tag{33}$$

The off-diagonal elements, for which popular algorithms use the Hadamard test for evaluation, can be evaluated in a much simpler fashion using the relationship

$$\mathrm{Re}[M_{\mu_i,\mu_j}] = M_{\mu_i+\mu_j,\mu_i+\mu_j} - \frac{M_{\mu_i,\mu_i}}{2} - \frac{M_{\mu_j,\mu_j}}{2} \tag{34}$$

where the term $M_{\mu_i+\mu_j,\mu_i+\mu_j}$ is given by

$$\begin{aligned}M_{\mu_i+\mu_j,\mu_i+\mu_j} = \langle 0|&\frac{1}{\sqrt{2}}(\hat{G}_{\mu_i} + \hat{G}_{\mu_j})^{\dagger}U(\theta)^{\dagger}\hat{H}U(\theta)\frac{1}{\sqrt{2}}\\ &(\hat{G}_{\mu_i} + \hat{G}_{\mu_j})|0\rangle\end{aligned} \tag{35}$$

The creation of entanglement $(\hat{G}_{\mu_i} + \hat{G}_{\mu_j})|0\rangle$ can be simply achieved by using a Hadamard gate along with a few CNOTs (maximum of seven CNOTs required).

The matrix elements of vector $\mathbf{Z}_Y$ can be similarly computed. All elements of this matrix are analogous to the off-diagonal elements of matrix **M**. It can be computed using the relationship

$$Z_{\mathrm{Y}}^{\mathrm{sc}}(\mu_i) = Z_{\mathrm{Y}}'(0{+}\mu_i) - \frac{Z_{\mathrm{Y}}'(\mu_i)}{2} - \frac{Z_Y'(0)}{2} \tag{36}$$

where

$$\begin{aligned} Z_{\mathrm{Y}}'(0 + \mu_i) &= \langle 0|\frac{1}{2}(\hat{I} + \hat{G}_{\mu_i})^\dagger U^\dagger(\theta)\hat{Y}U(\theta)\frac{1}{2}(\hat{I} + \hat{G}_{\mu_i})|0\rangle \\ Z_Y'(\mu_i) &= \langle 0|\hat{G}_{\mu_i{}^\dagger}U^\dagger(\theta)\hat{Y}U(\theta)\hat{G}_{\mu_i}|0\rangle \\ Z_Y'(0) &= \langle 0|U^\dagger(\theta)\hat{Y}U(\theta)|0\rangle \end{aligned} \tag{37}$$

The element $Z_Y'(0)$ can be computed once using the ground-state circuit, while the other two elements of Z_Y' needed for $Z^Y(\mu_i)$ can be evaluated separately for each element of the $\mathbf{Z}_\mathbf{Y}$ vector. The elements $Z_Y'(\mu_i)$ and $Z_Y'(0)$ can be computed by measuring the expectation value of operator $\hat{Y}$ using states $|\Psi_{\mu i}\rangle$ (see Figure 1a for an example) and $|\Psi_0\rangle$, respectively, where $|\Psi_X\rangle = U(\theta)\hat{G}_X|0\rangle$. The element $Z_Y{}'(0 + \mu_i)$ can be evaluated by measuring the expectation value of operator using state $|\Psi_{0+\mu i}\rangle$, which is prepared using a superposition of states $|0\rangle$ and $|\Psi_{\mu i}\rangle$ (see Figure 1b for an example).

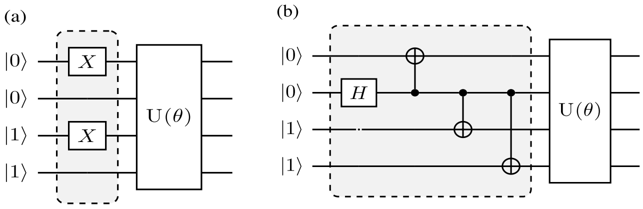

Figure 1. Proposed quantum circuit for the estimation of a representative element of the $\mathbf{Z}_\mathbf{Y}'$ vector element for using (a) an excited Slater determinant as the reference state and (b) an entangled state involving the HF state and excited Slater determinants as the reference state.

In the case of qLR(proj), the matrices $\mathbf{M}^{\mathbf{proj}}$, $\mathbf{V}^{\mathbf{proj}}$, and the vector $\mathbf{Z}_\mathbf{Y}^{\mathrm{proj}}$ in eq 32 can be computed using an estimate of RDMs using the prepared ground state. Evaluation of $\mathbf{M}^{\mathbf{proj}}$, $\mathbf{V}^{\mathbf{proj}}$, and $\mathbf{Z}^\mathbf{Y}$ will involve the estimation of up to six-, four-, and three-body RDMs, respectively.

The scaling of the shot count is dominated by the estimation of the matrix **M**, which scales as $O(N^{12})$ for both qLR(sc) and qLR(proj) approaches, where N is some measure of the system size. However, we can achieve a scaling reduction through making use of Hamiltonian factorization techniques,[79] and identifying the commuting products of Pauli operators appearing in the product of the Hamiltonian and excitation operators, and measure them simultaneously.[80] These requirements can be further reduced by utilizing commutators which lead to the cancellations of uncontracted terms,[81] approximations for higher-body RDMs, and taking advantage of the high symmetry of the **M** matrix (such as by the use of Krylov-subspace-based algorithms like the Davidson method). The pathways to reduce computational complexity will be a topic of later studies.

■ COMPUTATIONAL DETAILS

All of the calculations in this work employ the STO-3G basis set. The second-quantized Hamiltonian is generated by the PySCF[82] software package and transformed into the Pauli representation using the Jordon−Wigner mapping function of the OpenFermion[83] program. We use a state-vector simulator to test the accuracy of the methods developed in this work. The Fermionic ADAPT-VQE method[9] is employed to calculate the ground-state wave function using an operator pool composed of generalized singles and doubles excitation operators. Two classes of operator manifolds (self-consistent and projection operators that ensure that the VAC is always satisfied) are referred to in shorthand notation as sc and proj. Thus, the qEOM framework utilizing these operator manifolds is named as q-sc-EOM and q-proj-EOM. Similarly, we name the quantum formulation of linear response theory (qLR) using these operator manifolds as qLR(sc) and qLR(proj). In this work, the state-specific properties like excitation energies, oscillator strengths, and rotational strengths are evaluated

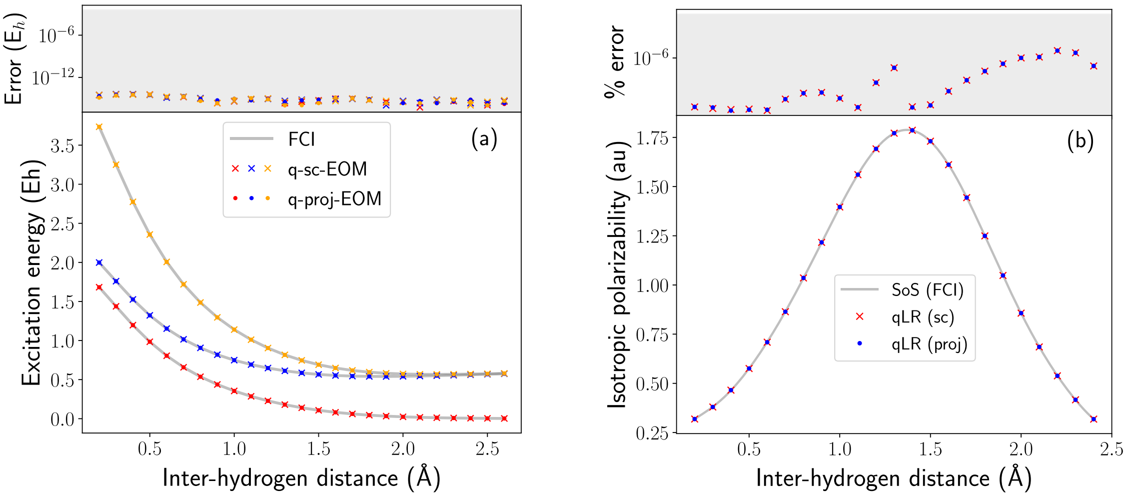

Figure 2. (a) Excitation energies (E_h) of the H_2 molecule calculated using the q-sc-EOM and q-proj-EOM approaches as a function of the interhydrogen distance and (b) isotropic dynamic electric-dipole polarizability of the H_2 molecule calculated at 589 nm using the qLR(sc) and qLR(proj) approaches as a function of the interhydrogen distance. The reference SoS(FCI) values are plotted in gray, and the deviations from the reference are shown in the upper panels, where the shaded region indicates errors below 0.1 eV in (a) and below 1% in (b).

https://doi.org/10.1021/acs.jctc.3c00731
J. Chem. Theory Comput. 2023, 19, 9136−9150

Table 1. Excitation Energy (E_{0k} in E_h), Overlap between the Ground and Excited States ($\langle 0|k\rangle$) and the Transition Dipole Moment in the z Direction ($\langle 0|\mu_z|k\rangle$, $e\ a_0$) for the Excited States of the H_2 Molecule at the Bond Length of 0.7 Å Obtained Using FCI, Q-sc-EOM, Q-proj-EOM, and qEOM Approaches with the STO-3G Basis Set

	FCI			q-sc-EOM			q-proj-EOM			qEOM		
states	E_{0k}	$\langle 0\|k\rangle$	$\langle 0\|\mu_z\|k\rangle$	E_{0k}	$\langle 0\|k\rangle$	$\langle 0\|\mu_z\|k\rangle$	E_{0k}	$\langle 0\|k\rangle$	$\langle 0\|\mu_z\|k\rangle$	E_{0k}	$\langle 0\|k\rangle$	$\langle 0\|\mu_z\|k\rangle$
T_0	0.6577	0	0	0.6577	0	0	0.6577	0	0	0.6577	0	0
S_1	1.0157	0	1.1441	1.0157	0	1.1441	1.0157	0	1.1441	1.0157	0	1.1441
S_2	1.7195	0	0	1.7195	0	0	1.7195	0	0	1.7195	0.1029	−0.1362

using the qEOM approaches (q-sc-EOM and q-proj-EOM), while dipole polarizabilities and specific rotation are calculated using the qLR theory [qLR(sc) and qLR(proj)]. It should be noted that all these approaches utilize the ground-state wave function obtained from the ADAPT-VQE algorithm with gradient convergence criteria set to 10^{-3} E_h. The code used for generating the data in this work can be found in ref 84.

RESULTS

H_2. The excitation energies (EEs) of the three excited states of the H_2 molecule using the STO-3G basis set are plotted in Figure 2a for both q-sc-EOM and q-proj-EOM approaches as a function of the interhydrogen distance. The reference full configuration interaction (FCI) EE values are plotted in gray, and the deviations in the EE values from the reference for both q-sc-EOM and q-proj-EOM methods are shown in the upper panel. It can be seen that the errors are less than 10^{-12} E_h across the entire potential energy curve. This is not surprising since the excitation manifold of singles and doubles used in this work spans a complete space for the H_2 molecule, and hence, both the methods are exact for a given basis set. Table 1 shows the excitation energy (E_{0k}), overlap between the ground and excited states ($\langle 0|k\rangle$) and the transition dipole moment in the z direction ($\langle 0|\mu_z|k\rangle$) of the H_2 molecule at a bond length of 0.7 Å, obtained using FCI, q-sc-EOM, q-proj-EOM and qEOM approaches. One can see that q-sc-EOM and q-proj-EOM approaches yield identical results to FCI but the qEOM method produces an incorrect value of the dipole transition moment for the S_2 excited state. The overlap between the ground state and the S_2 excited state is nonzero in the qEOM formalism, leading to the spurious value of the dipole transition moment. Rizzo and co-workers have also talked about the issue of nonorthogonality of ground and excited states in the qEOM approach in their work.[60] It should be noted that both q-sc-EOM and q-proj-EOM approaches satisfy the killer condition, which ensures that the ground and excited states are always orthogonal to each other, leading to a reliable and accurate simulation of the excited state properties. Figure 2b plots the dynamic isotropic electric dipole polarizability of the H_2 molecule calculated at 589 nm using the qLR(sc) and qLR(proj) approaches as a function of the interhydrogen distance. The reference values obtained using the SoS approach utilizing the FCI wave function are denoted as SoS(FCI) and are plotted in gray. The absolute percent errors of both approaches with respect to the reference SoS(FCI) values are shown in a log plot in the upper panel of the figure where the shaded region indicates errors below 1%. The isotropic polarizability is defined as the negative of one-third of the trace of the electric-dipole polarizability tensor. It can be easily seen that both qLR(sc) and qLR(proj) approaches produce essentially identical results, with errors always less than 10^{-6}%.

LiH. Figure 3a displays the dynamic electric-dipole polarizability of the LiH molecule calculated at 589 nm using the SoS(FCI) approach as a function of the Li−H bond distance. One can see the onset of the resonance when the Li−H distance is close to 2.7 and 3.4 Å. Unsurprisingly, the polarizability values approach infinity from positive and negative directions at these two points since the denominator in eq 14 becomes an infinitesimal quantity with both positive and negative signs around the point of resonance. One can verify this from Figure 3b where the excitation energies of the two lowest-lying excited states of the LiH molecule are plotted as a function of the Li−H distance. It can be seen that the excitation energy of the first singlet excited state (S_1) is equal to the frequency of light (589 nm) at around 2.7 and 3.4 Å. Of course, the triplet excited state is optically forbidden and does not contribute to the polarizability as the ground state is a singlet, resulting in a zero dipole transition moment. One can describe response properties in near-resonance regions through the help of damped RT.[85] However, this is beyond the scope of the current work where we are mostly concerned with calculation of response properties in nonresonant regions. Figure 4 plots the dynamic electric-dipole polarizability of the LiH molecule calculated at 589 nm using the qLR(sc) and qLR(proj) approaches as a function of the Li−H distance in

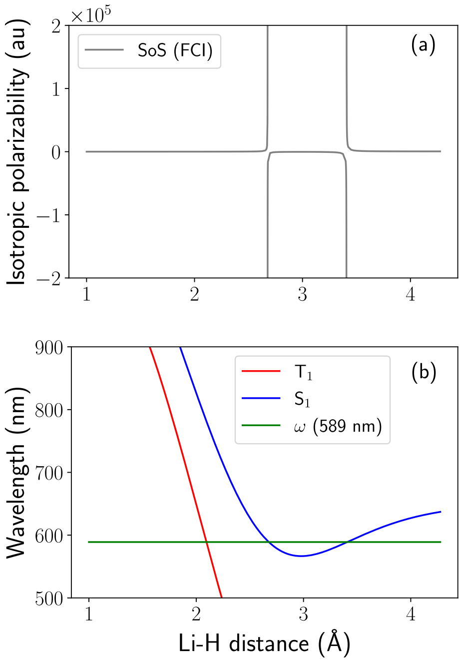

Figure 3. (a) Isotropic electric-dipole polarizability of the LiH molecule calculated at 589 nm using the SoS (FCI) approach. (b) Excitation energies of the two lowest-lying excited states of the LiH molecule, as a function of the Li−H distance.

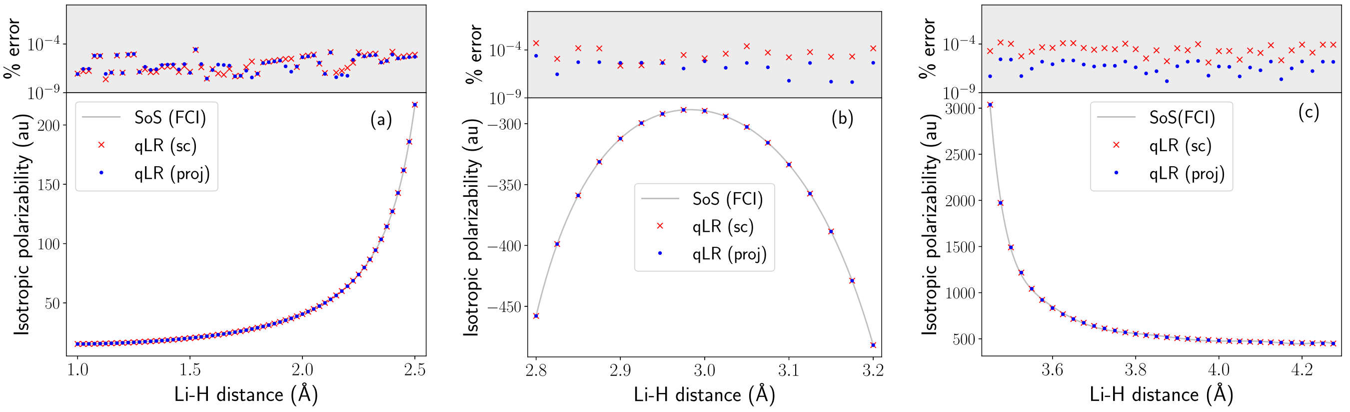

Figure 4. Isotropic dynamic electric-dipole polarizability of the LiH molecule calculated at 589 nm using the qLR(sc) and qLR(proj) approaches as a function of the Li−H distance in nonresonant regions (a,b,c). The reference SoS (FCI) values are plotted in gray, and the deviations from the reference are shown in the upper panel, where the shaded region indicates errors below 1%.

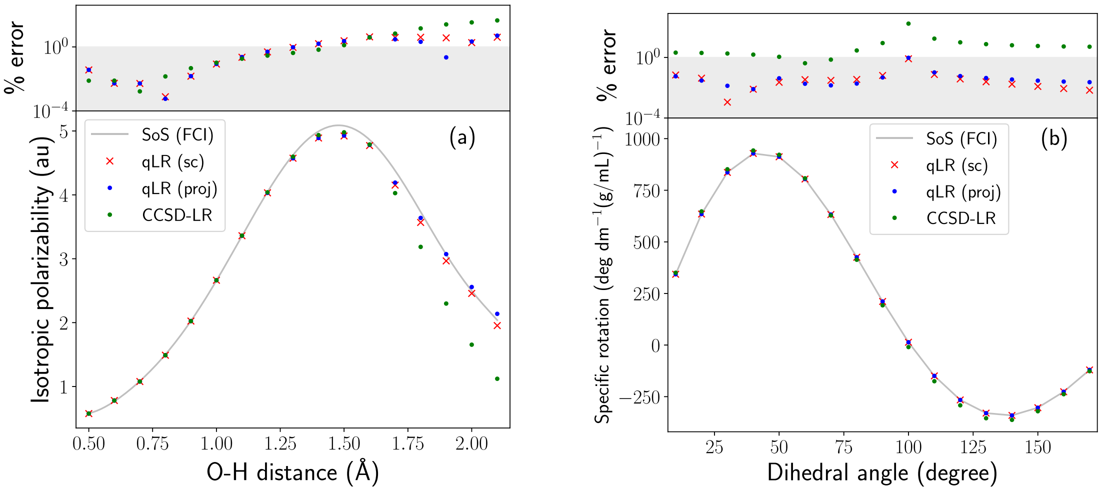

Figure 5. (a) Isotropic dynamic electric-dipole polarizability of the H_2O molecule calculated at 589 nm using the qLR(sc), qLR(proj), and CCSD-LR approaches as a function of the O−H bond distance. The reference SoS(FCI) values are plotted in gray and the deviations from the reference are shown in the upper panel, where the shaded region indicates errors below 1%. (b) Specific rotation of the helical $(H_2)_2$ molecule calculated at 589 nm using the qLR(sc), qLR(proj), and CCSD-LR approaches as a function of the H−H−H−H dihedral angle. The reference SoS(FCI) values are plotted in gray and the deviations from the reference are shown in the upper panel, where the shaded region indicates errors below 1%.

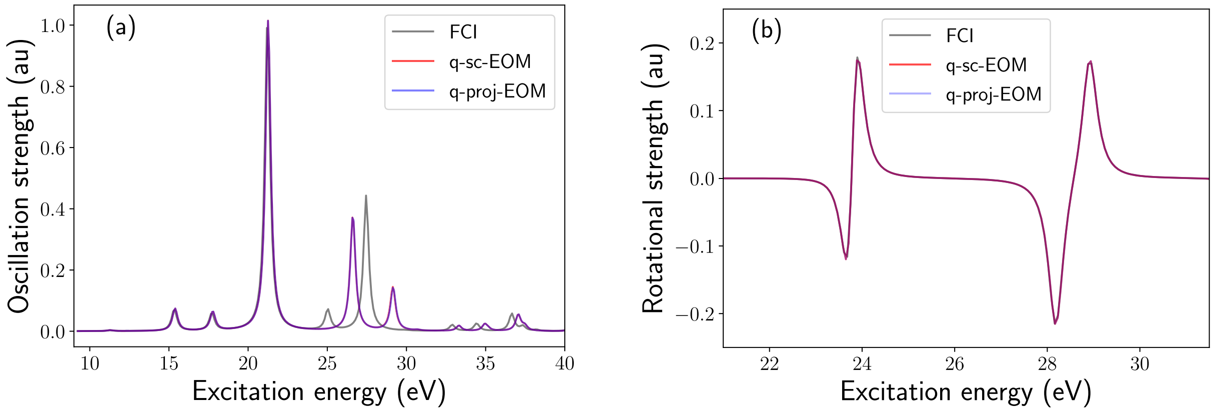

Figure 6. (a) UV−vis spectra of the H_2O molecule (equilibrium geometry) and (b) ECD spectra of the $(H_2)_2$ molecular system (dihedral angle = 100°), calculated using the FCI, q-sc-EOM, and q-proj-EOM approaches.

the three nonresonant regions of the potential energy spectrum. The reference SoS(FCI) values are plotted in gray, and the deviations from the reference are shown in the upper panel, where the shaded region indicates errors below 1%. It can be seen that the maximal absolute percent error is less than 10^{-3}% for both methods with the errors from the qLR(proj) approach slightly lower in magnitude.

H_2O. Figure 5a plots the dynamic electric-dipole polarizability of the H_2O molecule calculated at 589 nm using the quantum [qLR(sc), qLR(proj)] and classical (CCSD-LR) approaches as a function of the O−H bond distance. The reference values [SoS(FCI)] are plotted in gray, and the absolute percent errors of all three approaches with respect to the reference are shown in a log plot in the upper panel of the figure where the shaded region indicates errors below 1%. One can see that when the O−H bond distance is less than 1.5 Å, the errors produced by both quantum and classical approaches are close to 1%. This is because this region of the potential energy curve is characterized by weak electron correlation effects. As the O−H bond distance increases, strong correlation effects become dominant, and errors start to increase. For example, at an O−H bond distance of 2.1 Å, the errors from qLR(sc), qLR(proj), and CCSD-LR methods are close to 4, 5, and 45%, respectively. Thus, the quantum equation-of-motion approaches result in an order of magnitude reduction in the absolute percent error compared with the classical CCSD-LR method. This is due to the difference in the quality of the underlying ground-state wave function. The ADAPT-VQE procedure produces a ground-state wave function of similar quality to the FCI wave function, while the CCSD-LR method utilizes a CCSD ground-state wave function, which provides a very poor description of the electronic structure problem in the strong-correlation domain. It should be noted that all three approaches utilize only singles and doubles excitation operators to describe the time evolution of the ground-state wave function under an external time-dependent perturbation. Thus, we can reduce the errors in the quantum-response based approaches by including only a small set of higher-order excitation operators in the parameterization procedure due to the superior quality of the ground-state wave function. The left-hand plot in Figure 6a compares the UV−vis absorption spectra of the H_2O molecule at equilibrium geometry generated using FCI, q-sc-EOM, and q-proj-EOM approaches. The spectra produced by q-sc-EOM and q-proj-EOM are indistinguishable from one another and are in qualitative agreement with the FCI results.

$(H_2)_2$. The magnitude of the optical rotation of a chiral molecule is reflective of its detailed molecular structure and also depends on the frequency of the incident light. Optical rotation, when normalized for path length (dm) and concentration (g/mL), gives the specific rotation [deg dm^{-1} $(g/mL)^{-1}$] of the chiral medium. Figure 5b plots the specific rotation of the $(H_2)_2$ molecular system calculated at 589 nm using both quantum and classical methods (just like the H_2O molecule) as a function of the H−H−H−H dihedral angle. One can see that both the classical (CCSD-LR) and quantum methods produce results that are in qualitative agreement with the reference SoS(FCI) values. However, the errors produced by the classical CCSD-LR method are much larger than those of the quantum approaches across the entire dihedral angle curve. For example, when the dihedral angle is equal to 100°, the errors in qLR(sc), qLR(proj), and CCSD-LR approaches are 0.8%, 0.9%, and 170%, respectively. Furthermore, unlike the quantum approaches, the specific rotation curve produced by the CCSD-LR approach changes sign earlier compared to the reference curve. For example, the values of specific rotation at 100° calculated using SoS(FCI), qLR(sc), qLR(proj), and CCSD-LR approaches are 13.8, 13.7, 13.6, and −9.6°, respectively. It should be noted that the most important criterion for a specific rotation calculation is getting the sign correct. Thus, the quantum approaches offer a clear advantage over their classical counterparts in this regard. Absorption spectra (ECD and VCD) of chiral molecules can shed more light on the relationship between the molecular structure and the associated optical activity. Figure 6b compares the ECD absorption spectrum of the $(H_2)_2$ molecular system (H−H−H−H dihedral angle = 100°) generated using FCI, q-sc-EOM, and q-proj-EOM approaches. Just like the UV−vis spectra of the H_2O molecule, both q-sc-EOM and q-proj-EOM approaches produce identical spectra, which are in perfect agreement with the FCI values.

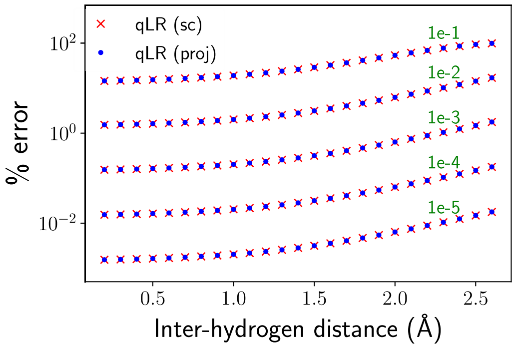

Figure 7. Percent error in isotropic electric dipole polarizability of the H_2 molecule at 589 nm for different values of errors (shown in green) in the optimized ground-state parameter, as a function of the interhydrogen distance for the qLR(sc) and qLR(proj) approaches.

Noise Analysis. In this subsection, we study the stability of qLR formalism to noise. We first investigate the propagation of errors from the ground-state VQE calculation to the isotropic electric-dipole polarizability of the H_2 molecule by introducing an error ϵ to the ground-state parameters ($\hat{\sigma}$), followed by a perturbative noise analysis to study the robustness of the above proposed algorithms for statistical errors (can be related to shot noise). Errors in the ground-state amplitudes ($\hat{\sigma}$) in any physically inspired ansatz can impact the calculated response properties. Figure 7 plots the absolute percent error in the isotropic electric-dipole polarizability of the H_2 molecule at 589 nm for different values of the errors (shown in green) in the optimized ground-state parameter, as a function of the interhydrogen distance for the qLR(sc) and qLR(proj) approaches using the STO-3G basis set. It can be seen that the percent errors in the isotropic electric-dipole polarizability are higher for every error value (10^{-1} to 10^{-5}) at larger interhydrogen distances. For the induced error of 10^{-3} in the ground-state amplitudes, the percent error is always less than 1%, while for 10^{-2}, the percent error stays always below 10%. In the perturbative noise analysis, we introduce an error from a uniform distribution within an error range (x axis) to each element of matrices M^{proj}, V^{proj}, and vector Z^{proj} in q-proj-EOM and M^{sc} and Z^{sc} in q-sc-EOM.[34]

Figure 8 plots the absolute percent error in the isotropic electric-dipole polarizability as a function of the error bounds for H_4 in a square planar geometry with a bond length of 1.5 Å. Each data point is an average over 10,000 separate calculations with randomly selected noise within the given bounds shown on the x-axis. One can see that the percent errors in the qLR(proj) approach can be much larger than the ones obtained in the qLR(sc) method. However, it cannot be

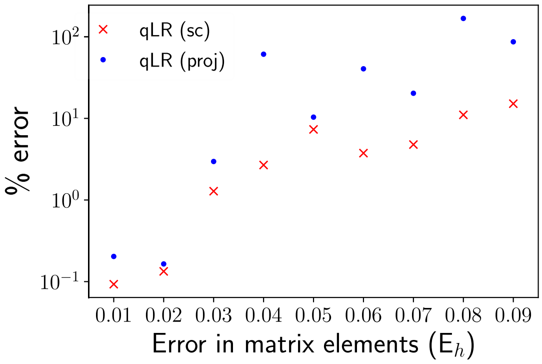

Figure 8. Percent error in isotropic electric dipole polarizability of the H_4 molecular system at 589 nm for the qLR(sc) and qLR(proj) approaches.

concluded that this trend will be true for a general molecular system.

We also carried out a noise sensitivity analysis of state-specific response properties such as excitation energies computed by using the quantum equation-of-motion framework and compared it with the QSE approach. In Figure 9a, we depict the sensitivity of the excitation energies of three lowest-lying excited states of a linear H_6 molecular system with a bond distance of 4 Å, computed using q-proj-EOM, q-sc-EOM, and QSE approaches, employing the same perturbative noise formalism as discussed above.

One can see that both QSE and q-proj-EOM methods are more sensitive to the noise compared with the q-sc-EOM formalism. Furthermore, the errors in the q-proj-EOM approach are lower than those of the QSE approach. It should be noted that the overlap matrix must be measured on a quantum computer in both the QSE and q-proj-EOM approaches. The measured overlap matrix with noise is then inverted to form an eigenvalue equation, a process that is sensitive to noise as discussed in ref 34. In Figure 9b, where we artificially eliminate all the noise in the overlap matrices of QSE and q-proj-EOM approaches, one can see very similar noise sensitivities of all three approaches. This demonstrates that the noise sensitivity of q-proj-EOM and QSE is a result of measuring the noisy overlap matrix. The overlap matrix in the q-sc-EOM approach on the other hand is exactly known (identity matrix), making this formalism quite noise-resilient. In future work, we plan to demonstrate the noise resilience of the q-sc-EOM and q-LR(sc) approaches on a real quantum device where we would like to employ quantum error mitigation strategies developed for VQE-based algorithms[11,86−88] to bring down the errors even further.

CONCLUSIONS

In this paper, we developed a new protocol for evaluating the molecular response properties on near-term quantum computers based on the linear-response framework, named qLR theory. Inspired by the recent work,[34,70,77] we make use of Mukherjee's self-consistent[64] (sc) and Surjáan's projected[65] (proj) excitation operator manifolds in conjunction with the qLR formalism to make sure that the "killer condition" is always satisfied. The two proposed formalisms, namely, qLR(sc) and qLR(proj), have been used for the evaluation of dipole polarizabilities and specific rotations of small molecular systems using the ground-state wave function obtained through the Fermionic ADAPT-VQE algorithm. We further test the newly developed methods, along with the analogous quantum equation-of-motion (qEOM) variants (q-sc-EOM and q-proj-EOM) to evaluate state-specific response properties such as excitation energies, oscillator strengths, and rotational strengths, which were then used to generate UV−vis and ECD spectra. Compared to the classical CCSD linear-response (CCSD-LR) theory, we find the quantum methods (without noise) significantly improve the accuracy of response properties near the strong correlation regions due to the better quality of the ground-state wave function. For example, for the chiral $(H_2)_2$ molecular system studied in this work, the specific rotation curve generated by the CCSD-LR theory changes sign earlier than the reference curve. This results in the wrong sign of the specific rotation at some geometric configurations. In contrast, the qLR approaches obtain the correct sign of specific rotation at every geometric configuration, with much smaller errors compared to the reference values. Furthermore, in the case of polarizabilities of the H_2O molecule, the qLR approaches produced an order of magnitude reduction in the errors compared to the CCSD-LR method in strongly correlated regions of the potential energy surface. The qLR formalism can also provide some insights toward the future development of UCC-based linear response approaches in classical quantum chemistry. Since response properties can be quite sensitive to the quality of basis sets, we also envision a combination of the qLR approach with the transcorrelated Hamiltonian formalism[89] in the future to obtain highly accurate properties using small basis sets. Thus, through this work, we demonstrate that quantum simulation of response properties using near-term quantum computers can be useful

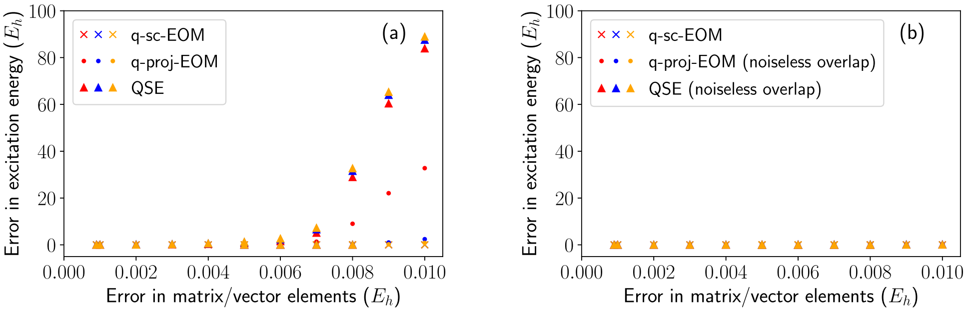

Figure 9. Sensitivity of excitation energies calculated as a function of errors in matrix elements in q-sc-EOM, q-proj-EOM, and QSE. In (a), errors are introduced in all matrices that are expected to be measured on a quantum computer. In (b), errors in the overlap matrix were not introduced in both the q-proj-EOM and QSE approaches.

in chemical sciences if the effects of noise are mitigated sufficiently.

■ APPENDIX

Expectation Value Picture of Response Functions

The first-order component of the Hamiltonian can be decomposed into the Fourier components as

$$\hat{H}^{(1)}(t) = \int_{-\infty}^{\infty} d\omega \hat{H}^{(1)}(\omega) e^{-i\omega t} \tag{A.1}$$

In the spirit of perturbation theory, the wavefunction can be expanded in different orders of the perturbation as

$$|\Psi_0(t)\rangle = |\Psi_0^{(0)}\rangle + |\Psi_0^{(1)}(t)\rangle + |\Psi_0^{(2)}(t)\rangle + \ldots \tag{A.2}$$

where the time-dependent perturbed wavefunction of a given order can be represented in terms of the Fourier transforms of their frequency-dependent counterparts, just like (A.A.1)

$$|\Psi_0^{(1)}(t)\rangle = \int_{-\infty}^{\infty} d\omega\; e^{-i\omega t} |\Psi_0^{(1)}(\omega)\rangle \tag{A.3}$$

$$|\Psi_0^{(2)}(t)\rangle = \int_{-\infty}^{\infty} d\omega_1 \int_{-\infty}^{\infty} d\omega_2\; e^{-i(\omega_1+\omega_2)t} |\Psi_0^{(2)}(\omega_1, \omega_2)\rangle$$

One can arrive at the closed expressions for response functions of different orders by expanding the time-dependent expectation value of a time-independent Hermitian operator $\hat{X}$ in orders of the perturbation $\hat{H}^{(1)}(t)$, e.g.,

$$\begin{aligned}\langle\hat{X}\rangle(t) = \langle\hat{X}\rangle^{(0)} + \int_{-\infty}^{\infty} d\omega \langle\langle\hat{X}; \hat{H}^{(1)}(\omega)\rangle\rangle \\ e^{-i\omega t} + \frac{1}{2}\int_{-\infty}^{\infty} d\omega_1 \int_{-\infty}^{\infty} d\omega_2 \langle\langle\hat{X}; \hat{\mathrm{H}}^{(1)}(\omega_1), \\ \hat{\mathrm{H}}^{(1)}(\omega_2)\rangle\rangle e^{-i(\omega_1+\omega_2)t} + \ldots\end{aligned} \tag{A.4}$$

where $\langle\hat{X}\rangle^{(0)}$ is the expectation value of the $\hat{X}$ operator with respect to the unperturbed time-independent ground-state wavefunction, $\langle\langle\hat{X}; \hat{H}^{(1)}(\omega)\rangle\rangle$ and $\langle\langle\hat{X}; \hat{\mathrm{H}}^{(1)}(\omega_1), \hat{\mathrm{H}}^{(1)}(\omega_2)\rangle\rangle$ refer to the linear and quadratic response functions, respectively, and so on. A response function of a given order in the presence of a given external field is associated with a specific physical phenomenon. For example, if $\hat{X}$ is the electric dipole operator, $\vec{\mu}$, and $\hat{H}^{(1)}(\omega)$ corresponds to an oscillating electric field, then the associated linear response function refers to the negative of the dynamic dipole polarizability (α) of the molecule, e.g.,

$$\langle\langle\hat{X}; \hat{H}^{(1)}(\omega)\rangle\rangle = \langle\langle\vec{\mu}; \vec{\mu}\rangle\rangle(\omega) = -\alpha(\omega) \tag{A.5}$$

If the perturbation is a magnetic field instead, then the imaginary part of the associated linear response function gives the Rosenfeld tensor, the trace of which is related to the optical rotation of the molecular system

$$\langle\langle\hat{X}; \hat{H}^{(1)}(\omega)\rangle\rangle = \langle\langle\vec{\mu}; \vec{m}\rangle\rangle(\omega) = G'(\omega) \tag{A.6}$$

where $\vec{m}$ corresponds to the magnetic moment operator.

EOM Theory

The EOM formalism[90] involves explicit evaluation of the excited states and the corresponding excitation energies and makes use of the sum of states approach (eq 14) to calculate the response properties. The wavefunction for the kth excited state ($|\Psi_k\rangle$) can be obtained by the action of a state-transfer operator ($\hat{\mathbb{O}}_k$) on the ground-state wavefunction ($|\Psi_0\rangle$)

$$|\Psi_k\rangle = \hat{\mathbb{O}}_k|\Psi_0\rangle \tag{B.1}$$

where $\hat{\mathbb{O}}_k$ has the same basic form as the time-dependent cluster operator (eq 7) in the linear response formalism

$$\hat{\mathbb{O}}_k = \sum_{i=1}^{N} \hat{R}_i^{\,k}$$

$$\hat{R}_i^{\,k} = \sum_{\mu} [A_{\mu_i}^{k}\hat{G}_{\mu_i} + B_{\mu_i^\dagger}^{k}\hat{G}_{\mu_i^\dagger}] \tag{B.2}$$

except that the coefficients $A_{\mu_i}^{k}$ and $B_{\mu_i^\dagger}^{k}$ are now time-independent and state-specific. Assuming the ground-state wavefunction and the state-transfer operator to be exact, the excitation energy associated with the transition from ground to kth excited state can be obtained through the application of a commutator of the Hamiltonian and the corresponding state-transfer operator on the ground-state wavefunction, which can be written as

$$[\hat{\mathrm{H}}, \hat{\mathbb{O}}_{\mathrm{k}}]|\Psi_0\rangle = \hat{\mathrm{H}}\hat{\mathbb{O}}_k|\Psi_0\rangle - \hat{\mathbb{O}}_k\hat{\mathrm{H}}|\Psi_0\rangle, = (E_k - E_0)\hat{\mathbb{O}}_k|\Psi_0\rangle \tag{B.3}$$

where E_0 and E_k are the energies of the ground and the kth excited state, respectively. Here, $\hat{H}$ refers to the molecular Hamiltonian operator in the second-quantized form. By projecting the above equation onto the kth excited-state wavefunction and assuming the VAC holds true (see The Vacuum Annihilation or "Killer" Condition section for details), one can compute the excitation energy directly as

$$E_{0k} = \frac{\langle\Psi_0|[(\hat{\mathbb{O}}_k^\dagger), [\hat{\mathrm{H}}, (\hat{\mathbb{O}}_k)]]|\Psi_0\rangle}{\langle\Psi_0|[(\hat{\mathbb{O}}_k^\dagger), (\hat{\mathbb{O}}_k)]|\Psi_0\rangle} \tag{B.4}$$

It can be seen that eq B.4 has a parametric dependence on the excitation ($A_{\mu_i}^{k}$) and de-excitation amplitudes ($B_{\mu_i^\dagger}^{k}$). By doing a variational minimization of the equation ($\delta E_{0k} = 0$), one can arrive at the following secular equation to solve for these amplitudes

$$\begin{pmatrix} \mathrm{M} & \mathrm{Q} \\ \mathbf{Q}^* & \mathbf{M}^* \end{pmatrix}\begin{pmatrix} \mathbf{A}^k \\ \mathbf{B}^k \end{pmatrix} = \mathrm{E}_{0\mathrm{k}}\begin{pmatrix} \mathrm{V} & \mathrm{W} \\ -\mathbf{W}^* & -\mathbf{V}^* \end{pmatrix}\begin{pmatrix} \mathbf{A}^k \\ \mathbf{B}^k \end{pmatrix} \tag{B.5}$$

where the expression for the matrix elements of **M**, **Q**, **V**, and **W** are the same as of eq 12. In this work, for computational convenience, we restrict the max rank of excitation and de-excitation operators to two, i.e., {i, j} ∈ {1, 2}. One is able to achieve "quantum advantage" through quantum measurements of these matrix elements since their classical evaluations will have a factorial scaling with respect to the system size for an exact ground-state wavefunction.

In this formalism, the ground-state wavefunction can be obtained in principle from any popular quantum algorithms. However, we employ the ADAPT-VQE procedure to obtain the ground-state wavefunction as it produces compact quantum circuits. Ollitrault and co-workers[33] developed and implemented this formalism on a quantum computer and named it as the "qEOM" method. Once the measurements are done, the generalized eigenvalue equation can be solved to obtain excitation energies, which possess the favorable property of size-intensivity. Furthermore, from the eigenvectors of eq B.5, one can calculate transition moments, which can be used to calculate the molecular absorption spectra. For example, to generate the ultraviolet−visible (UV−vis) spectra for a molecular system, one needs both excitation energies and oscillator strengths (OS) corresponding to different excited states where the OS gives the probability of an electric dipole transition from the ground state to a given excited state. Similarly, one can generate an ECD spectra for chiral molecules by calculating rotational strengths (RS) for different excited states. For the *k*th excited state, these quantities are defined as

$$\mathbf{OS}_k = \sum_i \frac{2}{3} \mathrm{E}_{0k}[\langle \Psi_0 | \vec{\boldsymbol{\mu}}_i | \Psi_k \rangle \langle \Psi_k | \vec{\boldsymbol{\mu}}_i | \Psi_0 \rangle$$

$$\mathbf{RS}_k = \sum_i [\langle \Psi_0 | \vec{\boldsymbol{\mu}}_i | \Psi_k \rangle \langle \Psi_k | \vec{\mathbf{m}}_i | \Psi_0 \rangle \tag{B.6}$$

where $i \in \{x, y, z\}$. Equation B.5 has a structure known as generalized random-phase approximation. In the context of quantum chemistry, this eigenvalue problem is frequently solved for TDHF or TDDFT methods. Of course, in TDHF (or TDDFT) approaches, only rank one excitations and de-excitations are considered, and the Hartee−Fock (or Kohn−Sham) determinant is taken as the reference wavefunction, while the matrices **M** and **Q** are commonly denoted as **A** and **B**.[91] Just like in the case of the TDHF/TDDFT formalism, one can encounter potential numerical issues while solving eq B.5 as it is not a generalized Hermitian eigenvalue problem.[92] One can always reformulate this equation into a generalized Hermitian eigenvalue equation to solve for $\mathbf{A}_k \pm \mathbf{B}_k$ instead, but the $\mathbf{M} - \mathbf{Q}$ matrix appearing in such a formulation would need to be strictly positive-definite, which might not be always guaranteed. Moreover, one needs to calculate inverse of $\mathbf{M} \pm \mathbf{Q}$ matrices, which could also cause potential numerical instabilities. One possible way to avoid this problem is by employing a Tamm−Dancoff (TDA)[92] like approximation and neglecting the de-excitation operators altogether. The QSE method does employ the TDA approximation and also includes identity in its operator pool, due to which the excitation energies obtained from QSE are not size-intensive.[93]

AUTHOR INFORMATION

Corresponding Authors

Ashutosh Kumar − *Theoretical Division, Los Alamos National Laboratory, Los Alamos, New Mexico 87545, United States*; orcid.org/0000-0001-7589-6030; Email: akumar1.quantum@gmail.com

Yu Zhang − *Theoretical Division, Los Alamos National Laboratory, Los Alamos, New Mexico 87545, United States*; orcid.org/0000-0001-8938-1927; Email: zhy@lanl.gov

Pavel A. Dub − *Chemistry Division, Los Alamos National Laboratory, Los Alamos, New Mexico 87545, United States*; Email: pdub@lanl.gov

Authors

Ayush Asthana − *Department of Chemistry, Virginia Tech, Blacksburg, Virginia 24061, United States*; orcid.org/0000-0002-7495-1867

Vibin Abraham − *Department of Chemistry, University of Michigan, Ann Arbor, Michigan 48109, United States*

T. Daniel Crawford − *Department of Chemistry, Virginia Tech, Blacksburg, Virginia 24061, United States*; orcid.org/0000-0002-7961-7016

Nicholas J. Mayhall − *Department of Chemistry, Virginia Tech, Blacksburg, Virginia 24061, United States*; orcid.org/0000-0002-1312-9781

Lukasz Cincio − *Theoretical Division, Los Alamos National Laboratory, Los Alamos, New Mexico 87545, United States*

Sergei Tretiak − *Theoretical Division, Los Alamos National Laboratory, Los Alamos, New Mexico 87545, United States; Center for Integrated Nanotechnologies, Los Alamos National Laboratory, Los Alamos, New Mexico 87545, United States*; orcid.org/0000-0001-5547-3647

Complete contact information is available at: https://pubs.acs.org/10.1021/acs.jctc.3c00731

Notes

The authors declare no competing financial interest.

ACKNOWLEDGMENTS

A.K., Y.Z., L.C., S.T., and P.A.D. thank the support from the Laboratory Directed Research and Development (LDRD) program of Los Alamos National Laboratory (LANL) under project number 20200056DR. LANL is operated by Triad National Security, LLC, for the National Nuclear Security Administration of the U.S. Department of Energy (contract no. 89233218CNA000001). A.A. and N.J.M. would like to acknowledge U.S. Department of Energy award no. DE-SC0019199. T.D.C. was supported by the U.S. National Science Foundation (grant CHE-2154753).

REFERENCES

(1) Evangelista, F. A. Perspective: Multireference coupled cluster theories of dynamical electron correlation. *J. Chem. Phys.* **2018**, *149* (3), 030901.

(2) Liu, J.; Cheng, L. Relativistic coupled-cluster and equation-of-motion coupled-cluster methods. *Wiley Interdiscip. Rev. Comput. Mol. Sci.* **2021**, *11* (6), No. e1536.

(3) Chan, G. K.-L.; Sharma, S. The density matrix renormalization group in quantum chemistry. *Annu. Rev. Phys. Chem.* **2011**, *62*, 465−481.

(4) Mardirossian, N.; Head-Gordon, M. Thirty years of density functional theory in computational chemistry: an overview and extensive assessment of 200 density functionals. *Mol. Phys.* **2017**, *115*, 2315−2372.

(5) Liu, G.; Zhang, C.; Ciborowski, S. M.; Asthana, A.; Cheng, L.; Bowen, K. H. Mapping the electronic structure of the uranium (VI) dinitride molecule, UN2. *J. Phys. Chem. A* **2020**, *124*, 6486−6492.

(6) Montgomery, J. M.; Mazziotti, D. A. Strong Electron Correlation in Nitrogenase Cofactor, FeMoco. *J. Phys. Chem. A* **2018**, *122*, 4988−4996.

(7) Nielsen, M. A.; Chuang, I. *Quantum Computation and Quantum Information*; Cambridge University Press: Cambridge, UK, 2011.

(8) Peruzzo, A.; McClean, J.; Shadbolt, P.; Yung, M.-H.; Zhou, X.-Q.; Love, P. J.; Aspuru-Guzik, A.; O'brien, J. L. A variational eigenvalue solver on a photonic quantum processor. *Nat. Commun.* **2014**, *5* (1), 4213.

(9) Grimsley, H. R.; Economou, S. E.; Barnes, E.; Mayhall, N. J. An adaptive variational algorithm for exact molecular simulations on a quantum computer. *Nat. Commun.* **2019**, *10* (1), 3007.

(10) Tang, H. L.; Shkolnikov, V.; Barron, G. S.; Grimsley, H. R.; Mayhall, N. J.; Barnes, E.; Economou, S. E. qubit-adapt-vqe: An adaptive algorithm for constructing hardware-efficient ansätze on a quantum processor. *PRX Quantum* **2021**, *2* (2), 020310.

(11) Kandala, A.; Mezzacapo, A.; Temme, K.; Takita, M.; Brink, M.; Chow, J. M.; Gambetta, J. M. Hardware-efficient variational quantum eigensolver for small molecules and quantum magnets. *Nature* **2017**, *549*, 242−246.

(12) Huggins, W. J.; Lee, J.; Baek, U.; O'Gorman, B.; Whaley, K. B. A non-orthogonal variational quantum eigensolver. *New J. Phys.* **2020**, *22* (7), 073009.

(13) Lee, J.; Huggins, W. J.; Head-Gordon, M.; Whaley, K. B. Generalized unitary coupled cluster wave functions for quantum computation. *J. Chem. Theory Comput.* **2019**, *15*, 311−324.

(14) Ryabinkin, I. G.; Yen, T.-C.; Genin, S. N.; Izmaylov, A. F. Qubit coupled cluster method: a systematic approach to quantum chemistry on a quantum computer. *J. Chem. Theory Comput.* **2018**, *14*, 6317−6326.

(15) O'Malley, P. J. J.; Babbush, R.; Kivlichan, I. D.; Romero, J.; McClean, J. R.; Barends, R.; Kelly, J.; Roushan, P.; Tranter, A.; Ding, N.; Campbell, B.; Chen, Y.; Chen, Z.; Chiaro, B.; Dunsworth, A.; Fowler, A. G.; Jeffrey, E.; Lucero, E.; Megrant, A.; Mutus, J. Y.; Neeley, M.; Neill, C.; Quintana, C.; Sank, D.; Vainsencher, A.; Wenner, J.; White, T. C.; Coveney, P. V.; Love, P. J.; Neven, H.; Aspuru-Guzik, A.; Martinis, J. M. Scalable quantum simulation of molecular energies. *Phys. Rev. X* **2016**, *6* (3), 031007.

(16) Nam, Y.; Chen, J.-S.; Pisenti, N. C.; Wright, K.; Delaney, C.; Maslov, D.; Brown, K. R.; Allen, S.; Amini, J. M.; Apisdorf, J.; Beck, K. M.; Blinov, A.; Chaplin, V.; Chmielewski, M.; Collins, C.; Debnath, S.; Hudek, K. M.; Ducore, A. M.; Keesan, M.; Kreikemeier, S. M.; Mizrahi, J.; Solomon, P.; Williams, M.; Wong-Campos, J. D.; Moehring, D.; Monroe, C.; Kim, J. Ground-state energy estimation of the water molecule on a trapped-ion quantum computer. *Npj Quantum Inf.* **2020**, *6* (1), 33.

(17) McCaskey, A. J.; Parks, Z. P.; Jakowski, J.; Moore, S. V.; Morris, T. D.; Humble, T. S.; Pooser, R. C. Quantum chemistry as a benchmark for near-term quantum computers. *Npj Quantum Inf.* **2019**, *5* (1), 99.

(18) Hempel, C.; Maier, C.; Romero, J.; McClean, J.; Monz, T.; Shen, H.; Jurcevic, P.; Lanyon, B. P.; Love, P.; Babbush, R.; Aspuru-Guzik, A.; Blatt, R.; Roos, C. F. Quantum chemistry calculations on a trapped-ion quantum simulator. *Phys. Rev. X* **2018**, *8* (3), 031022.

(19) Gao, Q.; Jones, G. O.; Motta, M.; Sugawara, M.; Watanabe, H. C.; Kobayashi, T.; Watanabe, E.; Ohnishi, Y.; Nakamura, H.; Yamamoto, N. Applications of quantum computing for investigations of electronic transitions in phenylsulfonyl-carbazole TADF emitters. *npj Comput. Mater.* **2021**, *7* (1), 70.

(20) Smart, S. E.; Mazziotti, D. A. Quantum solver of contracted eigenvalue equations for scalable molecular simulations on quantum computing devices. *Phys. Rev. Lett.* **2021**, *126* (7), 070504.

(21) Meitei, O. R.; Gard, B. T.; Barron, G. S.; Pappas, D. P.; Economou, S. E.; Barnes, E.; Mayhall, N. J. Gate-free state preparation for fast variational quantum eigensolver simulations. *Npj Quantum Inf.* **2021**, *7* (1), 155.

(22) Tkachenko, N. V.; Sud, J.; Zhang, Y.; Tretiak, S.; Anisimov, P. M.; Arrasmith, A. T.; Coles, P. J.; Cincio, L.; Dub, P. A. Correlation-Informed Permutation of Qubits for Reducing Ansatz Depth in the Variational Quantum Eigensolver. *PRX Quantum* **2021**, *2* (2), 020337.

(23) Zhang, Y.; Cincio, L.; Negre, C. F.; Czarnik, P.; Coles, P.; Anisimov, P. M.; Mniszewski, S. M.; Tretiak, S.; Dub, P. A. Variational Quantum Eigensolver with Reduced Circuit Complexity. *Npj Quantum Inf.* **2022**, *8* (1), 96.

(24) Asthana, A.; Liu, C.; Meitei, O. R.; Economou, S. E.; Barnes, E.; Mayhall, N. J. Minimizing state preparation times in pulse-level variational molecular simulations. arXiv preprint arXiv:2203.06818 **2022**, 1−12.

(25) Nakanishi, K. M.; Mitarai, K.; Fujii, K. Subspace-search variational quantum eigensolver for excited states. *Phys. Rev. Res.* **2019**, *1* (3), 033062.

(26) Xie, Q.-X.; Liu, S.; Zhao, Y. Orthogonal State Reduction Variational Eigensolver for the Excited-State Calculations on Quantum Computers. *J. Chem. Theory Comput.* **2022**, *18*, 3737−3746.

(27) Chan, H. H. S.; Fitzpatrick, N.; Segarra-Martí, J.; Bearpark, M. J.; Tew, D. P. Molecular excited state calculations with adaptive wavefunctions on a quantum eigensolver emulation: reducing circuit depth and separating spin states. *Phys. Chem. Chem. Phys.* **2021**, *23*, 26438−26450.

(28) Higgott, O.; Wang, D.; Brierley, S. Variational quantum computation of excited states. *Quantum* **2019**, *3* (1−11), 156.

(29) Colless, J. I.; Ramasesh, V. V.; Dahlen, D.; Blok, M. S.; Kimchi-Schwartz, M. E.; McClean, J. R.; Carter, J.; de Jong, W. A.; Siddiqi, I. Computation of molecular spectra on a quantum processor with an error-resilient algorithm. *Phys. Rev. X* **2018**, *8* (1), 011021.

(30) McClean, J. R.; Jiang, Z.; Rubin, N. C.; Babbush, R.; Neven, H. Decoding quantum errors with subspace expansions. *Nat. Commun.* **2020**, *11* (1), 636.

(31) Takeshita, T.; Rubin, N. C.; Jiang, Z.; Lee, E.; Babbush, R.; McClean, J. R. Increasing the Representation Accuracy of Quantum Simulations of Chemistry without Extra Quantum Resources. *Phys. Rev. X* **2020**, *10* (1), 011004.

(32) McClean, J. R.; Kimchi-Schwartz, M. E.; Carter, J.; De Jong, W. A. Hybrid quantum-classical hierarchy for mitigation of decoherence and determination of excited states. *Phys. Rev. A* **2017**, *95* (4), 042308.

(33) Ollitrault, P. J.; Kandala, A.; Chen, C.-F.; Barkoutsos, P. K.; Mezzacapo, A.; Pistoia, M.; Sheldon, S.; Woerner, S.; Gambetta, J. M.; Tavernelli, I. Quantum equation of motion for computing molecular excitation energies on a noisy quantum processor. *Phys. Rev. Res.* **2020**, *2* (4), 043140.

(34) Asthana, A.; Kumar, A.; Abraham, V.; Grimsley, H.; Zhang, Y.; Cincio, L.; Tretiak, S.; Dub, P. A.; Economou, S. E.; Barnes, E.; Mayhall, N. J. Quantum self-consistent equation-of-motion method for computing molecular excitation energies, ionization potentials, and electron affinities on a quantum computer. *Chem. Sci.* **2023**, *14*, 2405−2418.

(35) Abrams, D. S.; Lloyd, S. Quantum algorithm providing exponential speed increase for finding eigenvalues and eigenvectors. *Phys. Rev. Lett.* **1999**, *83*, 5162−5165.

(36) Aspuru-Guzik, A.; Dutoi, A. D.; Love, P. J.; Head-Gordon, M. Simulated quantum computation of molecular energies. *Science* **2005**, *309*, 1704−1707.

(37) Farhi, E.; Goldstone, J.; Gutmann, S.; Lapan, J.; Lundgren, A.; Preda, D. A quantum adiabatic evolution algorithm applied to random instances of an NP-complete problem. *Science* **2001**, *292*, 472−475.

(38) Babbush, R.; Love, P. J.; Aspuru-Guzik, A. Adiabatic quantum simulation of quantum chemistry. *Sci. Rep.* **2014**, *4* (1), 6603.

(39) Tkachenko, N. V.; Zhang, Y.; Cincio, L.; Boldyrev, A. I.; Tretiak, S.; Dub, P. A. Quantum Davidson Algorithm for Excited States. arxiv preprint arXiv:2204.10741 **2022**, 1−12.

(40) Motta, M.; Sun, C.; Tan, A. T. K.; O'Rourke, M. J.; Ye, E.; Minnich, A. J.; Brandão, F. G. S. L.; Chan, G. K.-L. Determining eigenstates and thermal states on a quantum computer using quantum imaginary time evolution. *Nat. Phys.* **2020**, *16*, 205−210.

(41) Stair, N. H.; Huang, R.; Evangelista, F. A. A Multireference Quantum Krylov Algorithm for Strongly Correlated Electrons. *J. Chem. Theory Comput.* **2020**, *16*, 2236−2245.

(42) Lane, N. The theory of electron-molecule collisions. *Rev. Mod. Phys.* **1980**, *52*, 29−119.

(43) Vela, A.; Gazquez, J. L. A relationship between the static dipole polarizability, the global softness, and the fukui function. *J. Am. Chem. Soc.* **1990**, *112*, 1490−1492.

(44) Hati, S.; Datta, D. Hardness and Electric Dipole Polarizability. Atoms and Clusters. *J. Phys. Chem.* **1994**, *98*, 10451−10454.

(45) Guo, H.; Gresh, N.; Roques, B. P.; Salahub, D. R. Many-body effects in systems of peptide hydrogen-bonded networks and their contributions to ligand binding: a comparison of the performances of DFT and polarizable molecular mechanics. *J. Phys. Chem. B* **2000**, *104*, 9746−9754.

(46) Wagnière, G. H. *Linear and Nonlinear Optical Properties of Molecules*; Wiley VCH: Basel, CH, 1993.

(47) Nguyen, L. A.; He, H.; Pham-Huy, C. Chiral Drugs: An Overview. *Int. J. Biomed. Sci.* **2006**, *2* (2), 85−100.

(48) Crawford, T. D. Ab initio calculation of molecular chiroptical properties. *Theor. Chem. Acc.* **2006**, *115*, 227−245.

(49) Koch, H.; Jørgensen, P. Coupled cluster response functions. *J. Chem. Phys.* **1990**, *93*, 3333−3344.

(50) Hirata, S.; Ivanov, S.; Bartlett, R. J.; Grabowski, I. Exact-exchange time-dependent density-functional theory for static and dynamic polarizabilities. *Phys. Rev. A* **2005**, *71* (3), 032507.

(51) Christiansen, O.; Jørgensen, P.; Hättig, C. Response functions from Fourier component variational perturbation theory applied to a time-averaged quasienergy. *Int. J. Quantum Chem.* **1998**, *68* (1), 1−52.

(52) Pedersen, T. B.; Koch, H. Coupled cluster response functions revisited. *J. Chem. Phys.* **1997**, *106*, 8059−8072.

(53) Stanton, J. F.; Bartlett, R. J. The equation of motion coupled-cluster method. A systematic biorthogonal approach to molecular excitation energies, transition probabilities, and excited state properties. *J. Chem. Phys.* **1993**, *98*, 7029−7039.

(54) Linderberg, J.; Öhrn, Y. *Propagators in Quantum Chemistry*; John Wiley & Sons: Hoboken, NJ, USA, 2004.

(55) Dreuw, A.; Wormit, M. The algebraic diagrammatic construction scheme for the polarization propagator for the calculation of excited states. *Wiley Interdiscip. Rev. Comput. Mol. Sci.* **2015**, *5*, 82−95.

(56) Huang, K.; Cai, X.; Li, H.; Ge, Z.-Y.; Hou, R.; Li, H.; Liu, T.; Shi, Y.; Chen, C.; Zheng, D.; Xu, K.; Liu, Z.-B.; Li, Z.; Fan, H.; Fang, W.-H. Variational Quantum Computation of Molecular Linear Response Properties on a Superconducting Quantum Processor. *J. Phys. Chem. Lett.* **2022**, *13*, 9114−9121.

(57) Cai, X.; Fang, W.-H.; Fan, H.; Li, Z. Quantum computation of molecular response properties. *Phys. Rev. Res.* **2020**, *2* (3), 033324.

(58) Abhishek; Singh, N.; Siwach, P.; Arumugam, P. A Quantum Algorithm for the Linear Response of Nuclei. arXiv preprint arXiv:2210.08757 **2022**, 1−18.

(59) Teplukhin, A.; Kendrick, B. K.; Mniszewski, S. M.; Zhang, Y.; Kumar, A.; Negre, C. F.; Anisimov, P. M.; Tretiak, S.; Dub, P. A. Computing molecular excited states on a D-Wave quantum annealer. *Sci. Rep.* **2021**, *11* (1), 18796.

(60) Rizzo, J.; Libbi, F.; Tacchino, F.; Ollitrault, P. J.; Marzari, N.; Tavernelli, I. One-particle Green's functions from the quantum equation of motion algorithm. arXiv preprint arXiv:2201.01826 **2022**, 1−10.

(61) Sawaya, N. P.; Huh, J. Improved resource-tunable near-term quantum algorithms for transition probabilities, with applications in physics and variational quantum linear algebra. arXiv preprint arXiv:2206.14213 **2022**, 1−13.

(62) Ibe, Y.; Nakagawa, Y. O.; Earnest, N.; Yamamoto, T.; Mitarai, K.; Gao, Q.; Kobayashi, T. Calculating transition amplitudes by variational quantum deflation. *Phys. Rev. Res.* **2022**, *4* (1), 013173.

(63) Cerezo, M.; Sone, A.; Volkoff, T.; Cincio, L.; Coles, P. J. Cost function dependent barren plateaus in shallow parametrized quantum circuits. *Nat. Commun.* **2021**, *12* (1), 1791.

(64) Prasad, M. D.; Pal, S.; Mukherjee, D. Some aspects of self-consistent propagator theories. *Phys. Rev. A* **1985**, *31*, 1287−1298.

(65) Szekeres, Z.; Szabados, Á.; Kállay, M.; Surján, P. R. On the "killer condition" in the equation-of-motion method: ionization potentials from multi-reference wave functions. *Phys. Chem. Chem. Phys.* **2001**, *3*, 696−701.

(66) Nooijen, M.; Shamasundar, K.; Mukherjee, D. Reflections on size-extensivity, size-consistency and generalized extensivity in many-body theory. *Mol. Phys.* **2005**, *103*, 2277−2298.

(67) Shavitt, I.; Bartlett, R. J. *Many-Body Methods in Chemistry and Physics: MBPT and Coupled-Cluster Theory*; Cambridge University Press: Cambridge, UK, 2009.

(68) We are mainly interested in calculating off-resonance response properties in this work. It should be noted that the damped version of response theory is used to calculate resonant response properties in classical quantum chemistry and one can easily extend the qLR theory along similar lines to simulate such properties on a quantum computer.

(69) Liu, J.; Asthana, A.; Cheng, L.; Mukherjee, D. Unitary coupled-cluster based self-consistent polarization propagator theory: A third-order formulation and pilot applications. *J. Chem. Phys.* **2018**, *148* (24), 244110.

(70) Fan, Y.; Liu, J.; Li, Z.; Yang, J. Equation-of-Motion Theory to Calculate Accurate Band Structures with a Quantum Computer. *J. Phys. Chem. Lett.* **2021**, *12*, 8833−8840.

(71) Sasagane, K.; Aiga, F.; Itoh, R. Higher-order response theory based on the quasienergy derivatives: The derivation of the frequency-dependent polarizabilities and hyperpolarizabilities. *J. Chem. Phys.* **1993**, *99*, 3738−3778.

(72) Wiberg, K. B.; Wang, Y.-g.; Wilson, S. M.; Vaccaro, P. H.; Cheeseman, J. R. Sum-over-states calculation of the specific rotations of some substituted oxiranes, chloropropionitrile, ethane, and norbornenone. *J. Phys. Chem. A* **2006**, *110*, 13995−14002.

(73) Mertins, F.; Schirmer, J.; Tarantelli, A. Algebraic propagator approaches and intermediate-state representations. II. The equation-of-motion methods for$N$,$N\pm1$, and$N\pm2$ electrons. *Phys. Rev. A* **1996**, *53*, 2153−2168.

(74) Weiner, B.; Goscinski, O. Calculation of optimal generalized antisymmetrized geminal-power (projected—Bardeen-Cooper-Schrieffer) functions and their associated excitation spectrum. *Phys. Rev. A* **1980**, *22*, 2374−2391.

(75) Hodecker, M.; Dreuw, A. Unitary coupled cluster ground-and excited-state molecular properties. *J. Chem. Phys.* **2020**, *153* (8), 084112.

(76) Levchenko, S. V.; Krylov, A. I. Equation-of-motion spin-flip coupled-cluster model with single and double substitutions: Theory and application to cyclobutadiene. *J. Chem. Phys.* **2004**, *120*, 175−185.

(77) Liu, J.; Fan, Y.; Li, Z.; Yang, J. Quantum algorithms for electronic structures: basis sets and boundary conditions. *Chem. Soc. Rev.* **2022**, *51*, 3263−3279.

(78) Kutzelnigg, W.; Shamasundar, K.; Mukherjee, D. Spinfree formulation of reduced density matrices, density cumulants and generalised normal ordering. *Mol. Phys.* **2010**, *108*, 433−451.

(79) Cohn, J.; Motta, M.; Parrish, R. M. Quantum Filter Diagonalization with Compressed Double-Factorized Hamiltonians. *PRX Quantum* **2021**, *2* (4), 040352.

(80) Yen, T.-C.; Ganeshram, A.; Izmaylov, A. F. Deterministic improvements of quantum measurements with grouping of compatible operators, non-local transformations, and covariance estimates. *npj Quantum Inf.* **2023**, *9* (1), 14.

(81) Liu, J.; Li, Z.; Yang, J. An efficient adaptive variational quantum solver of the Schrödinger equation based on reduced density matrices. *J. Chem. Phys.* **2021**, *154* (24), 244112.

(82) Sun, Q.; Berkelbach, T. C.; Blunt, N. S.; Booth, G. H.; Guo, S.; Li, Z.; Liu, J.; McClain, J. D.; Sayfutyarova, E. R.; Sharma, S.; Wouters, S.; Chan, G. K.-L. PySCF: the Python-based simulations of chemistry framework. *Wiley Interdiscip. Rev. Comput. Mol. Sci.* **2018**, *8* (1), No. e1340.

(83) McClean, J. R.; Rubin, N. C.; Sung, K. J.; Kivlichan, I. D.; Bonet-Monroig, X.; Cao, Y.; Dai, C.; Fried, E. S.; Gidney, C.; Gimby, B.; Gokhale, P.; Häner, T.; Hardikar, T.; Havlíček, V.; Higgott, O.; Huang, C.; Izaac, J.; Jiang, Z.; Liu, X.; McArdle, S.; Neeley, M.; O'Brien, T.; O'Gorman, B.; Ozfidan, I.; Radin, M. D.; Romero, J.; Sawaya, N. P. D.; Senjean, B.; Setia, K.; Sim, S.; Steiger, D. S.; Steudtner, M.; Sun, Q.; Sun, W.; Wang, D.; Zhang, F.; Babbush, R. OpenFermion: the electronic structure package for quantum computers. *Quantum Sci. Technol.* **2020**, *5* (3), 034014.

(84) Asthana, A.; Grimsley, H. R.; Kumar, A.; Abraham, V.; Mayhall, N. J. *Adapt-VQE*: https://github.com/asthanaa/adapt-vqe, 2022 GitHub repository.

(85) Kristensen, K.; Kauczor, J.; Kjærgaard, T.; Jørgensen, P. Quasienergy formulation of damped response theory. *J. Chem. Phys.* **2009**, *131* (4), 044112.

(86) Sagastizabal, R.; Bonet-Monroig, X.; Singh, M.; Rol, M. A.; Bultink, C. C.; Fu, X.; Price, C. H.; Ostroukh, V. P.; Muthusubramanian, N.; Bruno, A.; Beekman, M.; Haider, N.; O'Brien, T. E.; DiCarlo, L. Experimental error mitigation via symmetry verification in a variational quantum eigensolver. *Phys. Rev. A* **2019**, *100* (1), 010302.

(87) Temme, K.; Bravyi, S.; Gambetta, J. M. Error mitigation for short-depth quantum circuits. *Phys. Rev. Lett.* **2017**, *119* (18), 180509.

(88) Koczor, B. Exponential error suppression for near-term quantum devices. *Phys. Rev. X* **2021**, *11* (3), 031057.

(89) Kumar, A.; Asthana, A.; Masteran, C.; Valeev, E. F.; Zhang, Y.; Cincio, L.; Tretiak, S.; Dub, P. A. Quantum Simulation of Molecular Electronic States with a Transcorrelated Hamiltonian: Higher Accuracy with Fewer Qubits. *J. Chem. Theory Comput.* **2022**, *18*, 5312−5324.

(90) Rowe, D. Equations-of-motion method and the extended shell model. *Rev. Mod. Phys.* **1968**, *40*, 153−166.

(91) It should be noted that while the expressions for the matrix elements of A and B in TDHF is similar to eq 12, the TDDFT approach involves additional exchange-correlation correction.[93]

(92) Hirata, S.; Head-Gordon, M. Time-dependent density functional theory within the Tamm−Dancoff approximation. *Chem. Phys. Lett.* **1999**, *314*, 291−299.

(93) Hirata, S.; Head-Gordon, M. Time-dependent density functional theory for radicals: An improved description of excited states with substantial double excitation character. *Chem. Phys. Lett.* **1999**, *302*, 375−382.